
Transfer of Adversarial Robustness Between Perturbation Types

Daniel Kang^{*12} Yi Sun^{*13} Tom Brown¹ Dan Hendrycks⁴ Jacob Steinhardt¹

Abstract

We study the transfer of adversarial robustness of deep neural networks between different perturbation types. While most work on adversarial examples has focused on L_∞ and L_2 -bounded perturbations, these do not capture all types of perturbations available to an adversary. The present work evaluates 32 attacks of 5 different types against models adversarially trained on a 100-class subset of ImageNet. Our empirical results suggest that evaluating on a wide range of perturbation sizes is necessary to understand whether adversarial robustness transfers between perturbation types. We further demonstrate that robustness against one perturbation type *may not always* imply and may sometimes *hurt* robustness against other perturbation types. In light of these results, we recommend evaluation of adversarial defenses take place on a diverse range of perturbation types and sizes.

1. Introduction

Deep networks have shown remarkable accuracy on benchmark tasks (He et al., 2016), but can also be fooled by imperceptible changes to inputs, known as adversarial examples (Goodfellow et al., 2014). In response, researchers have studied the robustness of models, or how well models generalize in the presence of (potentially adversarial) bounded perturbations to inputs.

How can we tell if a model is robust? Evaluating model robustness is challenging because, while evaluating accuracy only requires a fixed distribution, evaluating the robustness of a model requires that the model have good performance in the presence of many, potentially hard to anticipate and model, perturbations. In the context of image classifica-

tion, considerable work has focused on robustness to “ L_∞ -bounded” perturbations (perturbations with bounded per-pixel magnitude) (Goodfellow et al., 2014; Madry et al., 2017; Xie et al., 2018). However, models hardened against L_∞ -bounded perturbations are still vulnerable to even small, perceptually minor departures from this family, such as small rotations and translations (Engstrom et al., 2017). Meanwhile, researchers continue to develop creative attacks that are difficult to even mathematically specify, such as fake eyeglasses, adversarial stickers, and 3D-printed objects (Sharif et al., 2018; Brown et al., 2017; Athalye et al., 2017).

The perspective of this paper is that any single, simple-to-define type of perturbation is likely insufficient to capture what a deployed model will be subject to in the real world. To address this, we investigate robustness of models with respect to a *broad range* of perturbation types. We start with the following question:

When and how much does robustness to one type of perturbation transfer to other perturbations?

We study this question using adversarial training, a strong technique for adversarial defense applicable to any fixed attack (Goodfellow et al., 2014; Madry et al., 2017). We evaluate 32 attacks of 5 different types— L_∞ (Goodfellow et al., 2014), L_2 (Carlini & Wagner, 2017), L_1 (Chen et al., 2018), elastic deformations (Xiao et al., 2018), and JPEG (Shin & Song, 2017)—against adversarially trained ResNet-50 models on a 100-class subset of full-resolution ImageNet.

Our results provide empirical evidence that models robust under one perturbation type *are not necessarily robust under other natural perturbation types*. We show that:

1. Evaluating on a carefully chosen range of perturbation sizes is important for measuring robustness transfer.
2. Adversarial training against the elastic deformation attack demonstrates that adversarial robustness against one perturbation type can transfer poorly to and at times hurt robustness to other perturbation types.
3. Adversarial training against the L_2 attack may be better than training against the widely used L_∞ attack.

While any given set of perturbation types may not encompass all potential perturbations that can occur in practice, our results demonstrate that robustness can fail to transfer even

^{*}Equal contribution, alphabetical ¹OpenAI, San Francisco, CA, USA ²Department of Computer Science, Stanford University, Palo Alto, CA, USA ³Department of Mathematics, Columbia University, New York, NY, USA ⁴Department of Electrical Engineering and Computer Science, UC Berkeley, Berkeley, CA, USA. Correspondence to: Daniel Kang <ddkang@stanford.edu>.

across a small but diverse set of perturbation types. Prior work in this area (Sharma & Chen, 2017; Jordan et al., 2019; Tramèr & Boneh, 2019) has studied transfer using single values of ε for each attack on lower resolution datasets; we believe our larger-scale study provides a more comprehensive and interpretable view on transfer between these attacks. We therefore suggest considering performance against several different perturbation types and sizes as a first step for rigorous evaluation of adversarial defenses.

2. Adversarial attacks

We consider five types of adversarial attacks under the following framework. Let $f : \mathbb{R}^{3 \times 224 \times 224} \rightarrow \mathbb{R}^{100}$ be a model mapping images to logits¹, and let $\ell(f(x), y)$ denote the cross-entropy loss. For an input x with true label y and a target class $y' \neq y$, the attacks attempt to find x' such that

1. the attacked image x' is a perturbation of x , constrained in a sense which differs for each attack, and
2. the loss $\ell(f(x'), y')$ is minimized (targeted attack).

We consider the targeted setting and the following attacks, described in more detail below:

- L_∞ (Goodfellow et al., 2014)
- L_2 (Szegedy et al., 2013; Carlini & Wagner, 2017)
- L_1 (Chen et al., 2018)
- JPEG
- Elastic deformation (Xiao et al., 2018)

The L_∞ and L_2 attacks are standard in the adversarial examples literature (Athalye et al., 2018; Papernot et al., 2016; Madry et al., 2017; Carlini & Wagner, 2017) and we chose the remaining attacks for diversity in perturbation type. We now describe each attack, with sample images in Figure 1 and Appendix A. We clamp output pixel values to $[0, 255]$.

For L_p attacks with $p \in \{1, 2, \infty\}$, the constraint allows an image $x \in \mathbb{R}^{3 \times 224 \times 224}$, viewed as a vector of RGB pixel values, to be modified to an attacked image $x' = x + \delta$ with

$$\|x' - x\|_p \leq \varepsilon,$$

where $\|\cdot\|_p$ denotes the L_p -norm on $\mathbb{R}^{3 \times 224 \times 224}$. For the L_∞ and L_2 attacks, we optimize using randomly-initialized projected gradient descent (PGD), which optimizes the perturbation δ by gradient descent and projection to the L_∞ and L_2 balls (Madry et al., 2017). For the L_1 attack, we use the randomly-initialized Frank-Wolfe algorithm (Frank & Wolfe, 1956), detailed in Appendix C. We believe that our Frank-Wolfe algorithm is more principled than the optimization used in existing L_1 attacks such as EAD.

¹For all experiments, the input is a 224×224 image, and the output is one of 100 classes.

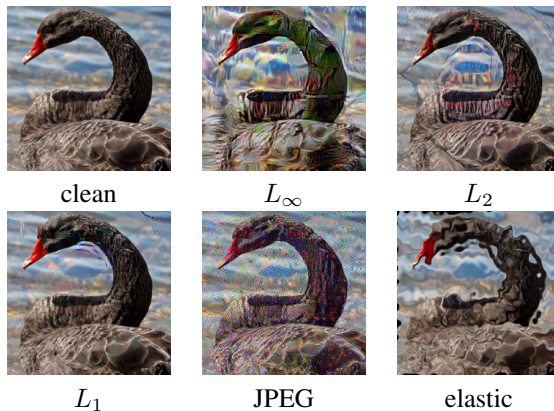


Figure 1. Sample attacked images with label “black swan” for ε at the top end of our range.

As discussed in Shin & Song (2017) as a defense, JPEG compression applies a lossy linear transformation based on the discrete cosine transform (denoted by JPEG) to image space, followed by quantization. The JPEG attack, which we believe is new to this work, imposes on the attacked image x' an L_∞ -constraint in this transformed space:

$$\|\text{JPEG}(x) - \text{JPEG}(x')\|_\infty \leq \varepsilon.$$

We optimize $z = \text{JPEG}(x')$ with randomly initialized PGD and apply a right inverse of JPEG to obtain the attacked image.

The elastic deformation attack allows perturbations

$$x' = \text{Flow}(x, V),$$

where $V : \{1, \dots, 224\}^2 \rightarrow \mathbb{R}^2$ is a vector field on pixel space, and Flow sets the value of pixel (i, j) to the (bilinearly interpolated) value at $(i, j) + V(i, j)$. We constrain V to be the convolution of a vector field W with a 25×25 Gaussian kernel with standard deviation 3, and enforce that

$$\|W(i, j)\|_\infty \leq \varepsilon \quad \text{for } i, j \in \{1, \dots, 224\}.$$

We optimize the value of W with randomly initialized PGD. Note that our attack differs in details from Xiao et al. (2018), but is similar in spirit.

3. Experiments

We measure transfer of adversarial robustness by evaluating our attacks against adversarially trained models. For each attack, we adversarially train models against the attack for a range of perturbation sizes ε . We then evaluate each adversarially trained model against each attack, giving the 2-dimensional accuracy grid of attacks evaluated against adversarially trained models shown in Figure 2 (analyzed in detail in Section 3.2).

Transfer of Adversarial Robustness Between Perturbation Types

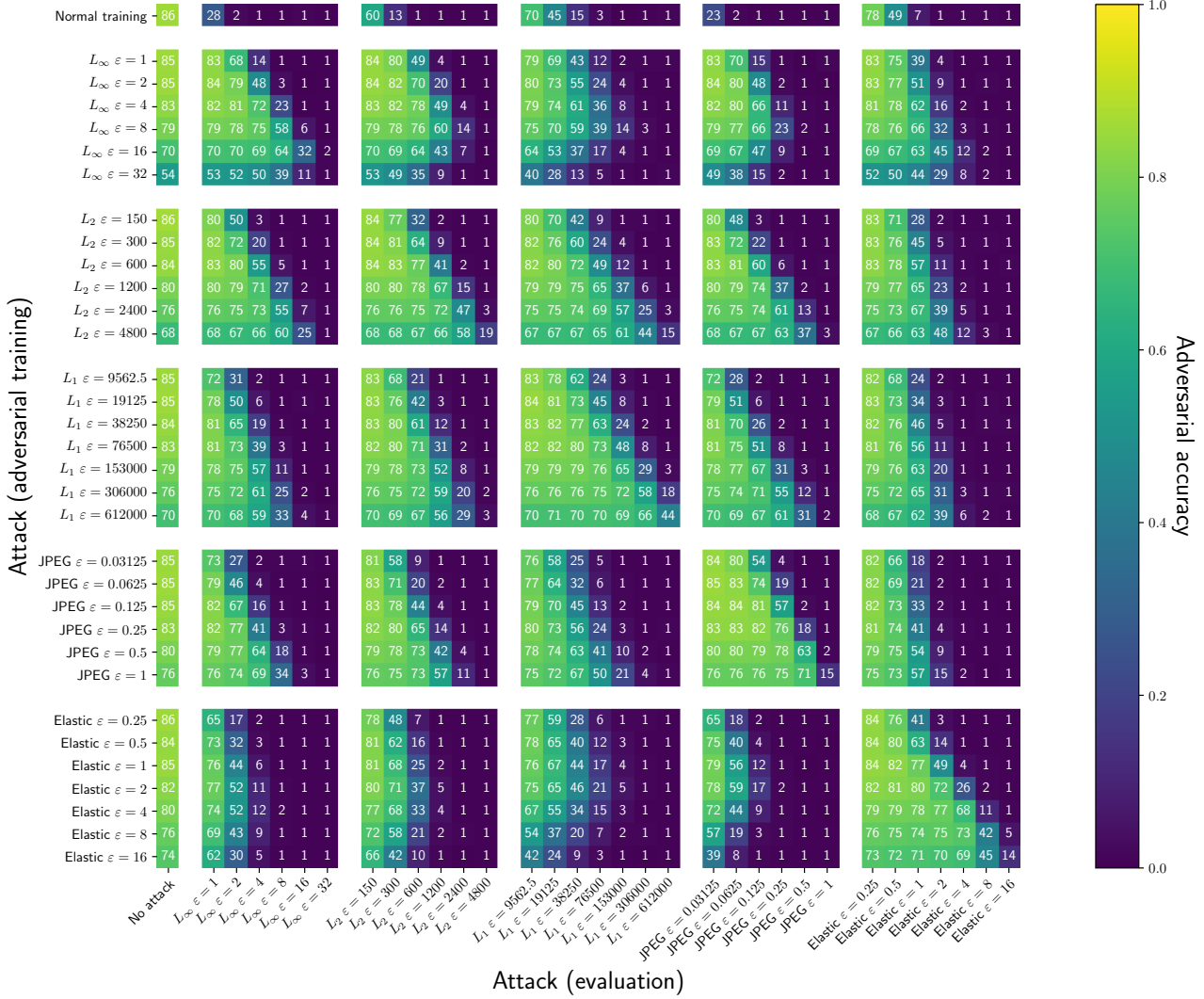


Figure 2. Evaluation accuracies of adversarial attacks (columns) against adversarially trained models (rows).

3.1. Experimental setup

Dataset and model. We use the 100-class subset of ImageNet-1K (Deng et al., 2009) containing classes whose WordNet ID is a multiple of 10. We use the ResNet-50 (He et al., 2016) architecture with standard 224×224 resolution as implemented in torchvision. We believe this full resolution is necessary for the elastic and JPEG attacks.

Training hyperparameters. We trained on machines with 8 Nvidia V100 GPUs using standard data augmentation practices (He et al., 2016). Following best practices for multi-GPU training (Goyal et al., 2017), we used synchronized SGD for 90 epochs with a batch size of 32×8 and a learning rate schedule in which the learning rate is “warmed up” for 5 epochs and decayed at epochs 30, 60, and 80 by a factor of 10. Our initial learning rate after warm-up was 0.1,

momentum was 0.9, and weight decay was 5×10^{-6} .

Adversarial training. We harden models against attacks using adversarial training (Madry et al., 2017). To train against attack A , for each mini-batch of training images, we select target classes for each image uniformly at random from the 99 incorrect classes. We generate adversarial images by applying the targeted attack A to the current model with ϵ chosen uniformly at random between 0 and ϵ_{\max} . Finally, we update the model with a step of synchronized SGD using these adversarial images alone.

We list attack parameters used for training in Table 1. For the PGD attack, we chose step size $\frac{\epsilon}{\sqrt{\text{steps}}}$, motivated by the fact that taking step size proportional to $1/\sqrt{\text{steps}}$ is optimal for non-smooth convex functions (Nemirovski & Yudin, 1978; 1983). Note that the greater number of PGD

Transfer of Adversarial Robustness Between Perturbation Types

attack	optimization algorithm	ε or ε_{\max} values	step size	steps (adversarial training)	steps (eval)
L_{∞}	PGD	$\{2^i \mid 0 \leq i \leq 5\}$	$\frac{\varepsilon}{\sqrt{\text{steps}}}$	10	50
L_2	PGD	$\{150 \cdot 2^i \mid 0 \leq i \leq 5\}$	$\frac{\varepsilon}{\sqrt{\text{steps}}}$	10	50
L_1	Frank-Wolfe	$\{9562.5 \cdot 2^i \mid 0 \leq i \leq 6\}$	N/A	10	50
JPEG	PGD	$\{0.03125 \cdot 2^i \mid 0 \leq i \leq 5\}$	$\frac{\varepsilon}{\sqrt{\text{steps}}}$	10	50
Elastic	PGD	$\{0.25 \cdot 2^i \mid 0 \leq i \leq 6\}$	$\frac{\varepsilon}{\sqrt{\text{steps}}}$	30	100

Table 1. Attack parameters for adversarial training and evaluation

steps for elastic deformation is due to the greater difficulty of its optimization problem, which we are not confident is fully solved even with this greater number of steps.

Attack hyperparameters. We evaluate our adversarially trained models on the (subsampled) ImageNet-1K validation set against targeted attacks with target chosen uniformly at random from among the 99 incorrect classes. We list attack parameters for evaluation in Table 1. As suggested in (Carlini et al., 2019), we use more steps for evaluation than for adversarial training to ensure PGD converges.

3.2. Results and analysis

Using the results of our adversarial training and evaluation experiments in Figure 2, we draw the following conclusions.

Choosing ε well is important. Because attack strength increases with the allowed perturbation magnitude ε , comparing robustness between different perturbation types requires a careful choice of ε for both attacks. First, we observe that a range of ε yielding comparable attack strengths should be used for all attacks to avoid drawing misleading conclusions. We suggest the following principles for choosing this range, which we followed for the parameters in Table 1:

1. Models adversarially trained against the minimum value of ε should have validation accuracy comparable to that of a model trained on unattacked data.
2. Attacks with the maximum value of ε should substantially reduce validation accuracy in adversarial training or perturb the images enough to confuse humans.

To illustrate this point, we provide in Appendix B a subset of Figure 2 with ε ranges that differ in strength between attacks; the (deliberately) biased ranges of ε chosen in this subset cause the L_1 and elastic attacks to be perceived as stronger than our full results reveal.

Second, even if two attacks are evaluated on ranges of ε of comparable strength, the specific values of ε chosen within those ranges may be important. In our experiments, we scaled ε geometrically for all attacks, but when interpreting our results, attack strength may not scale in the same way with ε for different attacks. As a result, we only draw conclusions which are invariant to the precise scaling of

attack strength with ε . We illustrate this type of analysis with the following two examples.

Robustness against elastic transfers poorly to the other attacks. In Figure 2, the accuracies of models adversarially trained against elastic are higher against elastic than the other attacks, meaning that for these values of ε , robustness against elastic does not imply robustness against other attacks. On the other hand, training against elastic with $\varepsilon \geq 4$ generally increases accuracy against elastic with $\varepsilon \geq 4$, but decreases accuracy against all other attacks.

Together, these imply that the lack of transfer we observe in Figure 2 is not an artifact of the specific values of ε we chose, but rather a broader effect at the level of perturbation types. In addition, this example shows that increasing robustness to larger perturbation sizes of a given type can hurt robustness to other perturbation types. This effect is only visible by considering an appropriate range of ε and cannot be detected from a single value of ε alone.

L_2 adversarial training is weakly better than L_{∞} . Comparing rows of Figure 2 corresponding to training against L_2 with $\varepsilon \in \{300, 600, 1200, 2400, 4800\}$ with rows corresponding to training against L_{∞} with $\varepsilon \in \{1, 2, 4, 8, 16\}$, we see that training against L_2 yields slightly lower accuracies against L_{∞} attacks and higher accuracies against all other attacks. Because this effect extends to all ε for which training against L_{∞} is helpful, it does not depend on the relation between L_{∞} attack strength and ε . In fact, against the stronger half of our attacks, training against L_2 with $\varepsilon = 4800$ gives comparable or better accuracy to training against L_{∞} with adaptive choice of ε . This provides some evidence that L_2 is more effective to train against than L_{∞} .

4. Conclusion

This work presents an empirical study of when and how much robustness transfers between different adversarial perturbation types. Our results on adversarial training and evaluation of 32 different attacks on a 100-class subset of ImageNet-1K highlight the importance of considering a diverse range of perturbation sizes and types for assessing transfer between types, and we recommend this as a guideline for evaluating adversarial robustness.

Acknowledgements

D. K. was supported by NSF Grant DGE-1656518. Y. S. was supported by a Junior Fellow award from the Simons Foundation and NSF Grant DMS-1701654. D. K., Y. S., and J. S. were supported by a grant from the Open Philanthropy Project.

References

- Athalye, A., Engstrom, L., Ilyas, A., and Kwok, K. Synthesizing robust adversarial examples. *CoRR*, abs/1707.07397, 2017. URL <http://arxiv.org/abs/1707.07397>.
- Athalye, A., Carlini, N., and Wagner, D. Obfuscated gradients give a false sense of security: Circumventing defenses to adversarial examples. *arXiv preprint arXiv:1802.00420*, 2018.
- Brown, T. B., Mané, D., Roy, A., Abadi, M., and Gilmer, J. Adversarial patch. *CoRR*, abs/1712.09665, 2017. URL <http://arxiv.org/abs/1712.09665>.
- Carlini, N. and Wagner, D. Towards evaluating the robustness of neural networks. In *2017 IEEE Symposium on Security and Privacy (SP)*, pp. 39–57. IEEE, 2017.
- Carlini, N., Athalye, A., Papernot, N., Brendel, W., Rauber, J., Tsipras, D., Goodfellow, I. J., Madry, A., and Kurakin, A. On evaluating adversarial robustness. *CoRR*, abs/1902.06705, 2019. URL <http://arxiv.org/abs/1902.06705>.
- Chen, P.-Y., Sharma, Y., Zhang, H., Yi, J., and Hsieh, C.-J. EAD: Elastic-net attacks to deep neural networks via adversarial examples. In *Thirty-second AAAI conference on artificial intelligence*, 2018.
- Deng, J., Dong, W., Socher, R., Li, L.-J., Li, K., and Fei-Fei, L. Imagenet: A large-scale hierarchical image database. In *2009 IEEE conference on computer vision and pattern recognition*, pp. 248–255. IEEE, 2009.
- Engstrom, L., Tran, B., Tsipras, D., Schmidt, L., and Madry, A. A rotation and a translation suffice: Fooling CNNs with simple transformations. *arXiv preprint arXiv:1712.02779*, 2017.
- Frank, M. and Wolfe, P. An algorithm for quadratic programming. *Naval research logistics quarterly*, 3(1-2): 95–110, 1956.
- Goodfellow, I. J., Shlens, J., and Szegedy, C. Explaining and harnessing adversarial examples. *arXiv preprint arXiv:1412.6572*, 2014.
- Goyal, P., Dollár, P., Girshick, R., Noordhuis, P., Wesolowski, L., Kyrola, A., Tulloch, A., Jia, Y., and He, K. Accurate, large minibatch SGD: Training Imagenet in 1 hour. *arXiv preprint arXiv:1706.02677*, 2017.
- He, K., Zhang, X., Ren, S., and Sun, J. Identity mappings in deep residual networks. In *European conference on computer vision*, pp. 630–645. Springer, 2016.
- Jordan, M., Manoj, N., Goel, S., and Dimakis, A. G. Quantifying Perceptual Distortion of Adversarial Examples. *arXiv e-prints*, art. arXiv:1902.08265, Feb 2019.
- Madry, A., Makelov, A., Schmidt, L., Tsipras, D., and Vladu, A. Towards deep learning models resistant to adversarial attacks. *arXiv preprint arXiv:1706.06083*, 2017.
- Nemirovski, A. and Yudin, D. On Cezari’s convergence of the steepest descent method for approximating saddle point of convex-concave functions. In *Soviet Math. Dokl*, volume 19, pp. 258–269, 1978.
- Nemirovski, A. and Yudin, D. *Problem Complexity and Method Efficiency in Optimization*. Intersci. Ser. Discrete Math. Wiley, New York, 1983.
- Papernot, N., McDaniel, P., Wu, X., Jha, S., and Swami, A. Distillation as a defense to adversarial perturbations against deep neural networks. In *2016 IEEE Symposium on Security and Privacy (SP)*, pp. 582–597. IEEE, 2016.
- Sharif, M., Bhagavatula, S., Bauer, L., and Reiter, M. K. Adversarial generative nets: Neural network attacks on state-of-the-art face recognition. *CoRR*, abs/1801.00349, 2018. URL <http://arxiv.org/abs/1801.00349>.
- Sharma, Y. and Chen, P.-Y. Attacking the Madry Defense Model with L_1 -based Adversarial Examples. *arXiv e-prints*, art. arXiv:1710.10733, Oct 2017.
- Shin, R. and Song, D. JPEG-resistant adversarial images. In *NIPS 2017 Workshop on Machine Learning and Computer Security*, 2017.
- Szegedy, C., Zaremba, W., Sutskever, I., Bruna, J., Erhan, D., Goodfellow, I., and Fergus, R. Intriguing properties of neural networks. *arXiv preprint arXiv:1312.6199*, 2013.
- Tramèr, F. and Boneh, D. Adversarial Training and Robustness for Multiple Perturbations. *arXiv e-prints*, art. arXiv:1904.13000, Apr 2019.
- Xiao, C., Zhu, J.-Y., Li, B., He, W., Liu, M., and Song, D. Spatially transformed adversarial examples. *arXiv preprint arXiv:1801.02612*, 2018.
- Xie, C., Wu, Y., van der Maaten, L., Yuille, A., and He, K. Feature denoising for improving adversarial robustness. *arXiv preprint arXiv:1812.03411*, 2018.

A. Sample attacked images

In this appendix, we give more comprehensive sample outputs for our adversarial attacks. Figures 3 and 4 show sample attacked images for attacks with relatively large and small ε in our range, respectively. Figure 5 shows examples of how attacked images can be influenced by different types of adversarial training for defense models. In all cases, the images were generated by running the specified attack against an adversarially trained model with parameters specified in Table 1 for both evaluation and adversarial training.

B. Evaluation on a truncated ε range

In this appendix, we show in Figure 6 a subset of Figure 2 with a truncated range of ε . In particular, we omitted small values of ε for L_1 , elastic, and JPEG and large values of ε for L_∞ and L_2 . The resulting accuracy grid gives several misleading impressions, including:

1. The L_1 attack is stronger than L_∞ , L_2 , and JPEG.
2. Training against the other attacks gives almost no robustness against the elastic attack.

The full range of results in Figure 2 shows that these two purported effects are artifacts of the incorrectly truncated range of ε used in Figure 6. In particular:

1. The additional smaller ε columns for the L_1 attack in Figure 2 demonstrate its perceived strength in Figure 6 is an artifact of incorrectly omitting these values.
2. The additional smaller ε columns for the elastic attack in Figure 2 reveal that training against the other attacks is effective in defending against weak versions of the elastic attack, contrary to the impression given by Figure 6.

C. L_1 Attack

We chose to use the Frank-Wolfe algorithm for optimizing the L_1 attack, as Projected Gradient Descent would require projecting onto a truncated L_1 ball, which is a complicated operation. In contrast, Frank-Wolfe only requires optimizing linear functions $g^\top x$ over a truncated L_1 ball; this can be done by sorting coordinates by the magnitude of g and moving the top k coordinates to the boundary of their range (with k chosen by binary search). This is detailed in Algorithm 1.

Transfer of Adversarial Robustness Between Perturbation Types

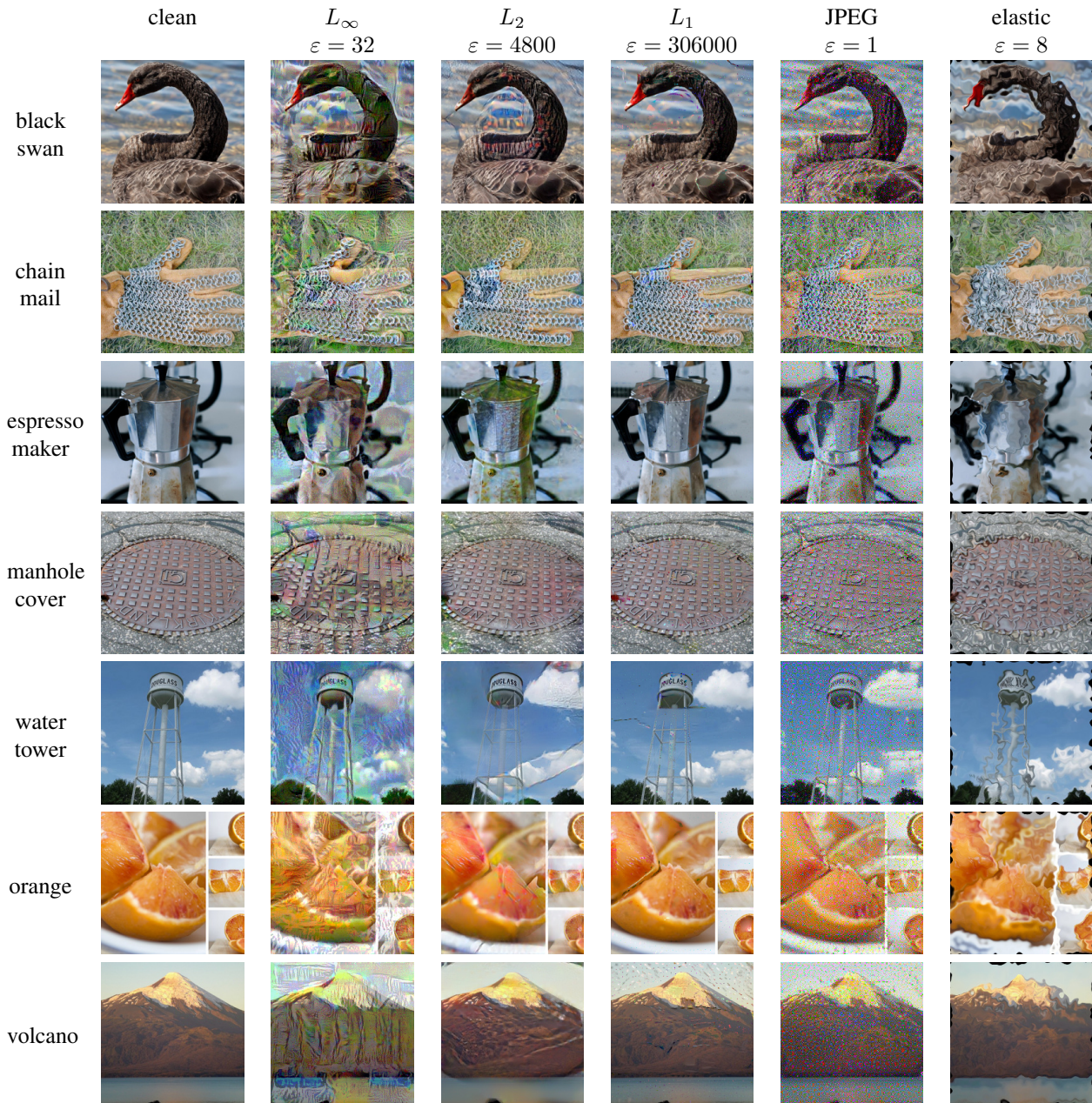


Figure 3. Strong attacks applied to sample images

Transfer of Adversarial Robustness Between Perturbation Types

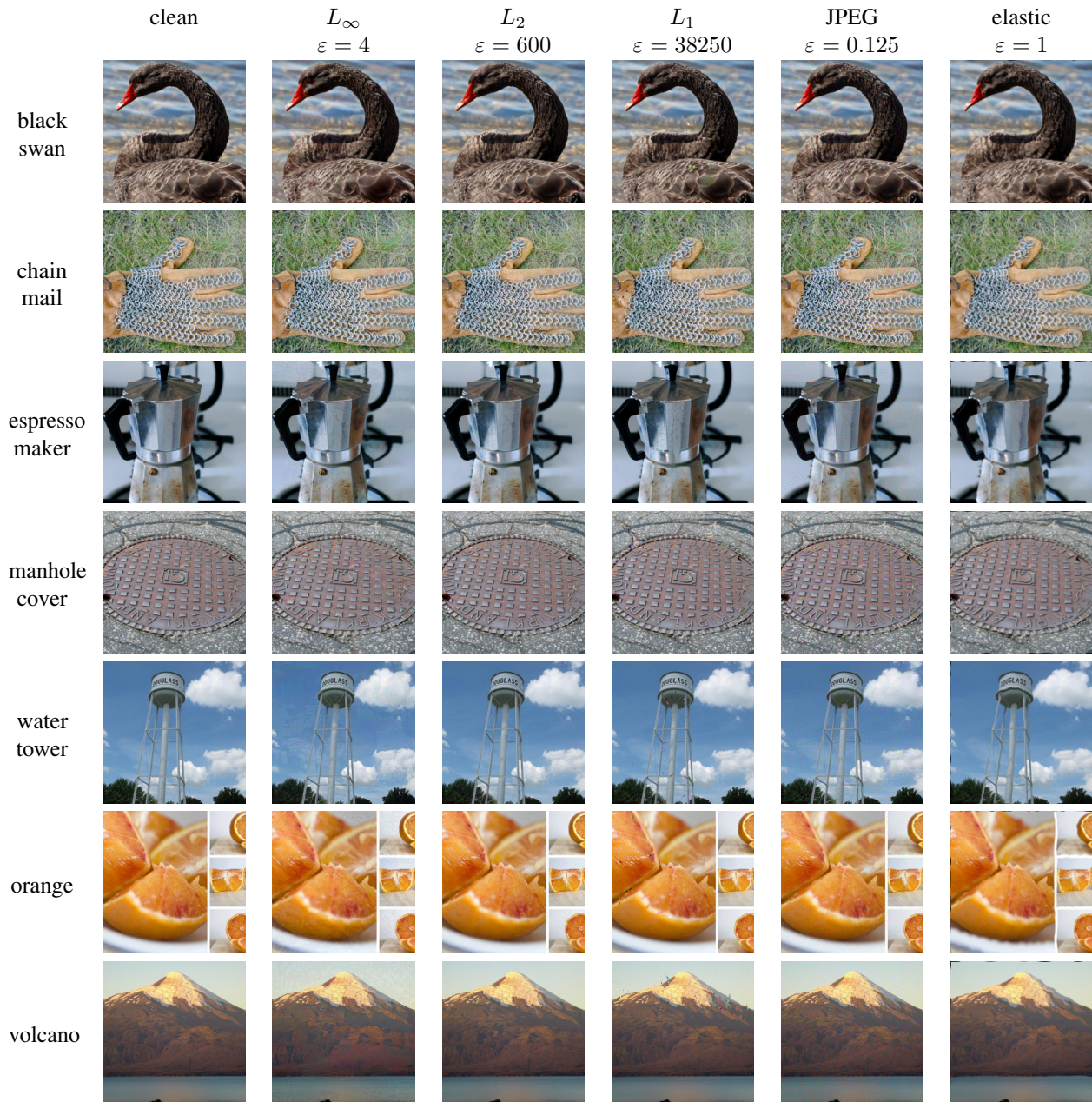


Figure 4. Weak attacks applied to sample images

Transfer of Adversarial Robustness Between Perturbation Types

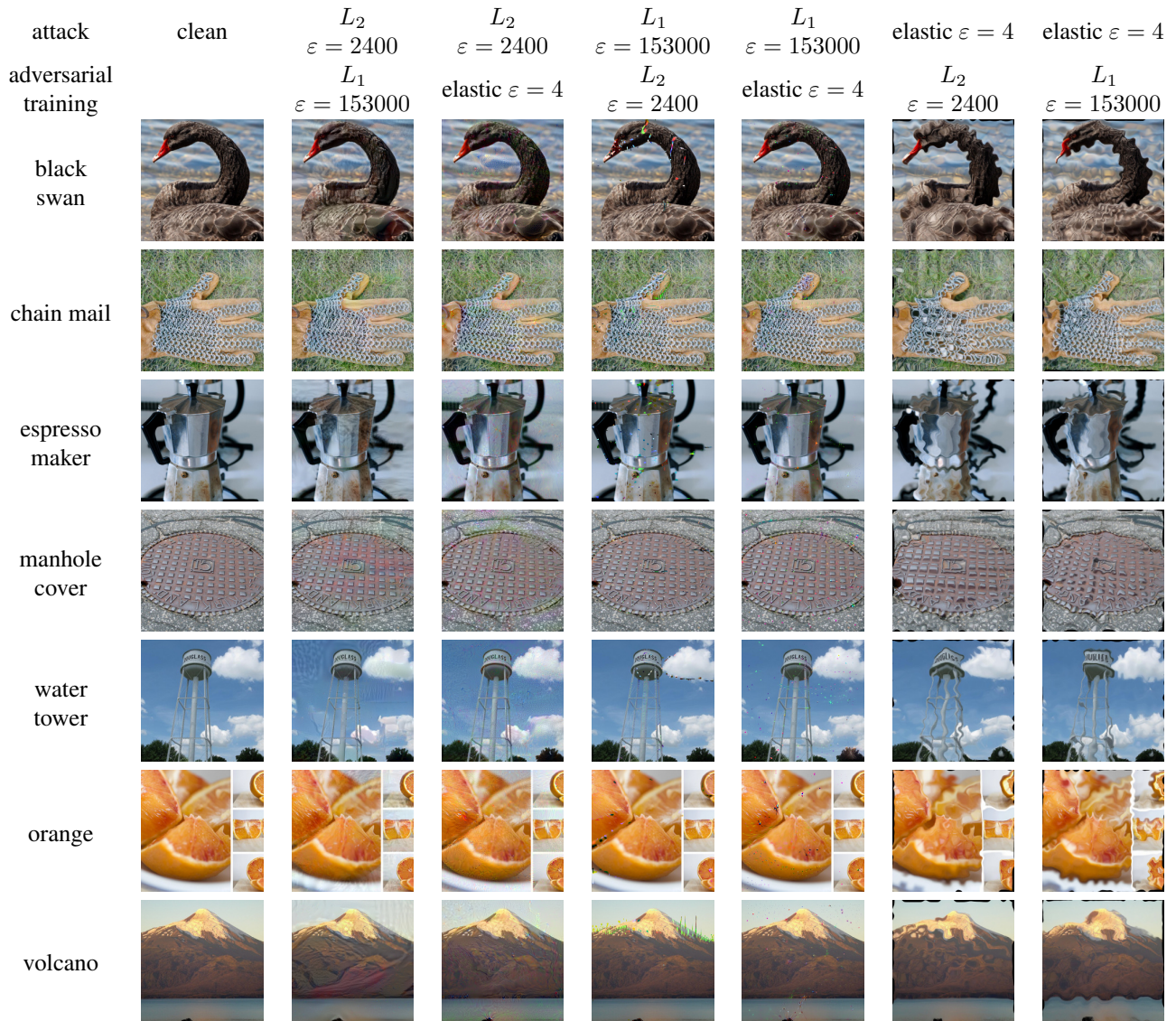


Figure 5. Transfer across attack types

Transfer of Adversarial Robustness Between Perturbation Types

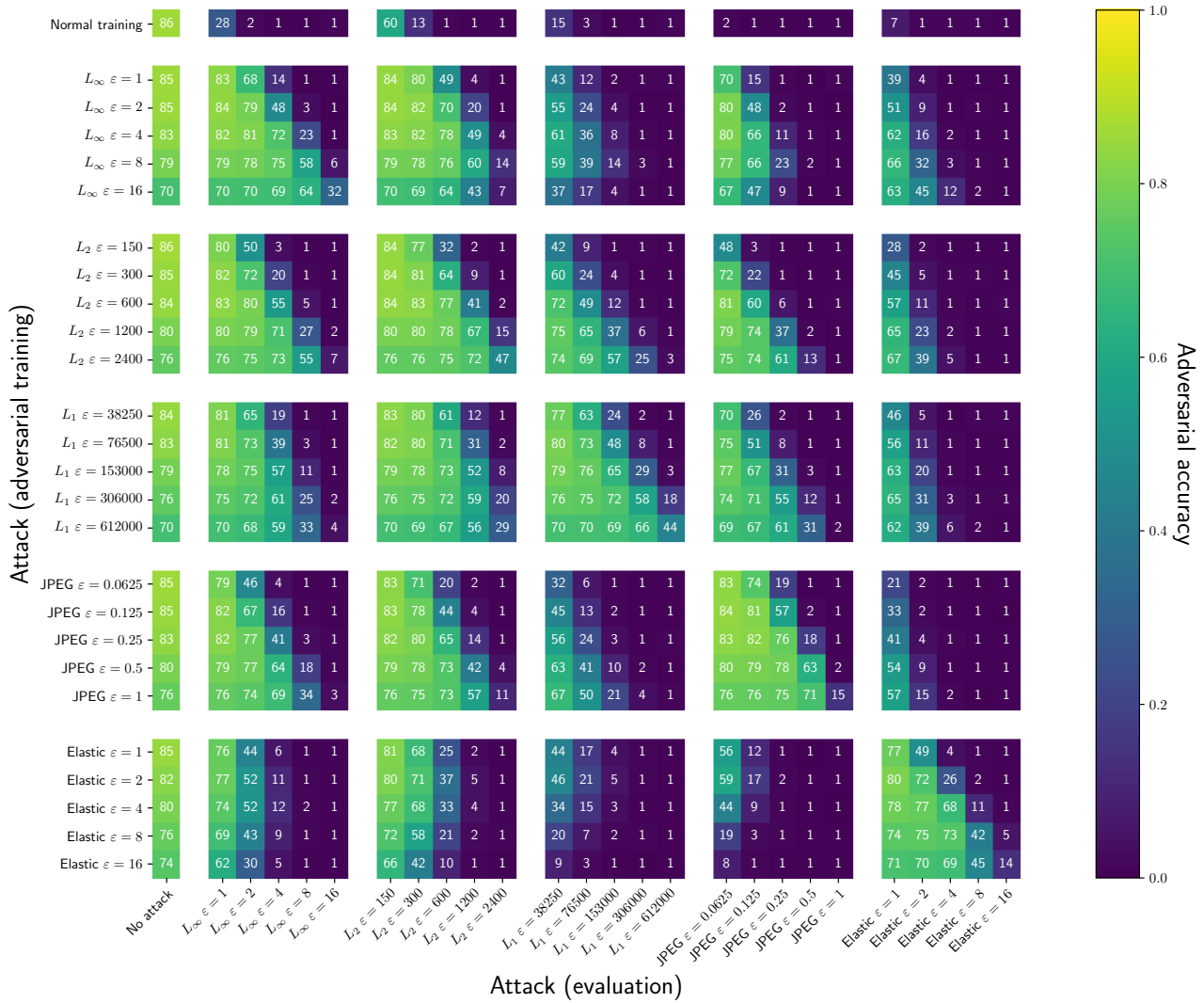


Figure 6. Evaluation accuracies of adversarial attacks (columns) against adversarially trained models (rows) for a truncated ϵ range.

Algorithm 1 Pseudocode for the Frank-Wolfe algorithm for the L_1 attack.

```

1: Input: function  $f$ , initial input  $x \in [0, 1]^d$ ,  $L_1$  radius  $\rho$ , number of steps  $T$ .
2: Output: approximate maximizer  $\bar{x}$  of  $f$  over the truncated  $L_1$  ball  $B_1(\rho; x) \cap [0, 1]^d$  centered at  $x$ .
3:
4:  $x^{(0)} \leftarrow \text{RandomInit}(x)$  ▷ Random initialization
5: for  $t = 1, \dots, T$  do
6:    $g \leftarrow \nabla f(x^{(t-1)})$  ▷ Obtain gradient
7:   for  $k = 1, \dots, d$  do
8:      $s_k \leftarrow$  index of the coordinate of  $g$  by with  $k^{\text{th}}$  largest norm
9:   end for
10:   $S_k \leftarrow \{s_1, \dots, s_k\}$ .
11:
12:  for  $i = 1, \dots, d$  do ▷ Compute move to boundary of  $[0, 1]$  for each coordinate.
13:    if  $g_i > 0$  then
14:       $b_i \leftarrow 1 - x_i$ 
15:    else
16:       $b_i \leftarrow -x_i$ 
17:    end if
18:  end for
19:   $M_k \leftarrow \sum_{i \in S_k} |b_i|$  ▷ Compute  $L_1$ -perturbation of moving  $k$  largest coordinates.
20:   $k^* \leftarrow \max\{k \mid M_k \leq \rho\}$  ▷ Choose largest  $k$  satisfying  $L_1$  constraint.
21:  for  $i = 1, \dots, d$  do ▷ Compute  $\hat{x}$  maximizing  $g^\top x$  over the  $L_1$  ball.
22:    if  $i \in S_{k^*}$  then
23:       $\hat{x}_i \leftarrow x_i + b_i$ 
24:    else if  $i = s_{k^*+1}$  then
25:       $\hat{x}_i \leftarrow x_i + (\rho - M_{k^*}) \text{sign}(g_i)$ 
26:    else
27:       $\hat{x}_i \leftarrow x_i$ 
28:    end if
29:  end for
30:   $x^{(t)} \leftarrow (1 - \frac{1}{t})x^{(t-1)} + \frac{1}{t}\hat{x}$  ▷ Average  $\hat{x}$  with previous iterates
31: end for
32:  $\bar{x} \leftarrow x^{(T)}$ 

```
